Chen *et al. Cancer Nanotechnology* (2023) 14:78
https://doi.org/10.1186/s12645-023-00230-6

Cancer Nanotechnology

RESEARCH Open Access

Targeting and internalizing PEGylated nanodrugs to enhance the therapeutic efficacy of hematologic malignancies by anti-PEG bispecific antibody (mPEG × CD20)

Huei-Jen Chen[1,2], Yi-An Cheng[1], Yu-Tung Chen[2], Chia-Ching Li[2], Bo-Cheng Huang[1,3], Shih-Ting Hong[2], I.-Ju Chen[3,12], Kai-Wen Ho[3], Chiao-Yun Chen[3,5,6], Fang-Ming Chen[7,8,9], Jaw-Yuan Wang[3], Steve R. Roffler[2,10], Tian-Lu Cheng[1,3,4*] and Dung-Ho Wu[11*]

*Correspondence:
tlcheng5024@gmail.com;
wudungho@mail.cnu.edu.tw

[1] Department of Biomedical Science and Environmental Biology, Kaohsiung Medical University, 100 Shih-Chuan 1st Road, Kaohsiung 80708, Taiwan
[11] Chia Nan University of Pharmacy and Science, 60 Section 1, Erren Rd, Rende District, Tainan 71710, Taiwan
Full list of author information is available at the end of the article

Abstract

Background: PEGylated nanoparticles (PEG-NPs) are not effective for hematologic malignancies as they lack the enhanced permeability and retention effect (EPR effect). Tumor-targeted PEG-NPs can systemically track lymphoma and actively internalize into cancer cells to enhance therapeutic efficacy. We generated an anti-PEG bispecific antibody (BsAb; mPEG × CD20) which was able to simultaneously bind to methoxy PEG on liposomes and CD20 to form multivalent αCD20-armed liposomes. This αCD20-armed liposome was able to crosslink CD20 on lymphoma cells to enhance cellular internalization and the anti-cancer efficacy of the liposomes to lymphoma. We generated mPEG × CD20 and used this bispecific antibody to modify PEGylated liposomal doxorubicin (PLD) through a one-step formulation.

Results: αCD20-armed PLD (αCD20/PLD) specifically targeted $CD20^+$ Raji cells and enhanced PLD internalization 56-fold after 24 h. αCD20/PLD also increased cytotoxicity to Raji cells by 15.2-fold in comparison with PLD and control mPEG × DNS-modified PLD (αDNS/PLD). mPEG × CD20 significantly enhanced the tumor accumulation 2.8-fold in comparison with mPEG × DNS-conjugated PEGylated liposomal DiD in Raji tumors. Moreover, αCD20/PLD had significantly greater therapeutic efficacy as compared to αDNS/PLD ($P < 0.0001$) and PLD($P < 0.0001$), and αCD20/PLD-treated mice had a 90% survival rate at 100-day post-treatment.

Conclusions: Modification of mPEG × CD20 can confer PLD with CD20 specificity to enhance the internalization and the anti-cancer efficacy of PEG-NPs. This therapeutic strategy can conveniently be used to modify various PEG-NPs with anti-PEG BsAb to overcome the lack of EPR effect of hematologic malignancies and improve therapeutic efficacy.

Keywords: PEGylated nanoparticles (PEG-NPs), Enhanced permeability and retention effect (EPR effect), Anti-PEG bispecific antibody (BsAb; mPEG × CD20), CD20-armed liposomes, αCD20/PLD, Hematologic malignancies

Introduction

Non-Hodgkin's lymphoma (NHL) is a type of hematologic malignancy that accounts for at least 90% of lymphoma cases, which presents not only as a solid tumor of lymphoid cells in lymph nodes and/or extranodal lymphatic organs, but also as free lymphoma cells in circulating blood (Wu et al. 2014; Jiang et al. 2016). Patients with high-grade B-cell NHL, such as diffuse large cell B-cell lymphoma (DLBCL), may require treatment with high-dose CHOP (cyclophosphamide, doxorubicin, vincristine, and prednisone) chemotherapy (Rivankar et al. 2014) and immunotherapy using monoclonal antibodies, such as rituximab (Jiang et al. 2016; Huwyler et al. 2008). However, about 30–50% of patients are not cured by this treatment (Coiffier et al. 2010; Coiffier and Sarkozy 2016). One of the limitations is the toxicity of CHOP, such as immune pancytopenia, that is caused by high-dose chemotherapy that not only eliminates lymphoma but also harms the normal blood cells in the spleen and bone marrow (Nagashima et al. 2016; Chatterjee et al. 2010; Franco et al. 2018). About 5% of patients older than age 60 years die because of R-CHOP toxicity (Jardin et al. 2019). Thus, reducing the systemic toxicity of chemotherapy drugs can improve the therapeutic efficacy of lymphoma treatment. PEGylated nanoparticles (PEG-NP) are a promising formulation for reducing the systemic toxicity of chemotherapy drugs, because liposomes can reduce exposure of normal cells to a high concentration of the chemotherapy drugs upon intravenous administration. In the clinic, the PEGylated liposomal doxorubicin (PLD; Caelyx® and Lipo-Dox®) has been shown to have low cardiotoxicity for treatment of patients with B-DLCL (Zaja et al. 2006; Milla et al. 2012; Suk et al. 2016; Da-Silva-Freitas et al. 2015), and only 4% (3/79) of elderly patients with B-DLCL had grade 3 cardiac events (Oki et al. 2015). However, there is currently no convincing evidence for the anti-cancer effect of PLD treatment in hematologic malignancies (Murawski et al. 2010; García-Noblejas, et al. 2018). Possible reasons for this are the lack of EPR effect in circulating tumors to reduce the tumor accumulation of PEGylated liposomes, and the hydrophilic PEG moiety hindering cellular uptake of liposomes (Khan et al. 2015). Therefore, there is a need to develop PEG-NPs that have more tumor specificity and active transport into cells to improve the therapeutic efficacy in B-cell NHL.

Conjugation of antibodies on PEG-NP can induce endocytosis of the NP into tumor cells to enhance therapeutic efficacy. For example, Jiang and colleagues conjugated anti-CD20 antibody on active carbon nanoparticles (ACNP) through the amine group of the antibody, and the anti-CD20 ACNP had a fivefold increase in cytotoxicity to Raji cells (Jiang et al. 2016; Tsimberidou et al. 2010). Using reducing agent to activate the Fab fragments of rituximab for reactivity toward the maleimide on adriamycin-loading liposome, they proved that anti-CD20 Fab liposome could significantly prolong the survival of mice ($P < 0.05$) (Wu et al. 2014). However, chemical conjugation may influence the binding activity of antibodies (Sapra et al. 2002). Antibodies have several functional groups (amine, carboxyl, thiol groups) resulting in heterogeneous coupling orientations (Manjappa et al. 2011; Bendas et al. 1999). Additionally, the reducing agent which generates cysteine residues can in turn cause additional damage and loss of antibody stability (Nobs et al. 2004; Hammer et al. 2007; Shahum et al. 1998; Trubetskoy et al. 1992; Zhang et al. 2016). Therefore, it is important that the modification method is convenient and does not add harmful substances to retain the

stability of antibodies and targeted particles. We have developed anti-mPEG bispecific antibodies (BsAb; mPEG × marker), which can directly and rapidly attach to the surface of PEG-NP with a non-covalent bond to confer specific targeting to PEG-NPs. A one-step formulation of mPEG × HER2 or mPEG × EGFR increased tumor accumulation of PEG-NP by 175% and 208% in HER2- or EGFR-positive solid tumors, respectively (Cheng et al. 2019; Cheng et al. 2020; Kao et al. 2014).

To easily create nanomedicines that can target CD20-expressing hematologic malignancies lacking the EPR effect, we generated a humanized bispecific antibody (BsAb; mPEG × CD20) composed of a humanized anti-mPEG Fab linked to a human anti-CD20 single-chain antibody (scFv). The BsAb can target the terminal methoxy groups present on PEG chains surrounding PLD to confer CD20 specificity (αCD20/PLD) by a one-step formulation. The αCD20/PLD enhances the targeting, internalization, and anti-cancer activity in CD20-expressing hematologic malignancies (Fig. 1). In this study, we investigated the specific targeting and the internalization of αCD20/PLD when incubated with $CD20^+$ Raji cells. We then evaluated whether αCD20/PLD enhances the cytotoxicity of PLD. Finally, we investigated the tumor accumulation and therapeutic efficacy of αCD20/PLD in mice bearing Raji tumors. We have thus found a new treatment for hematologic malignancies, by a one-step formulation of PEG-NPs with mPEG × CD20 to target lymphoma and enhance the internalization and the therapeutic efficacy of PLD.

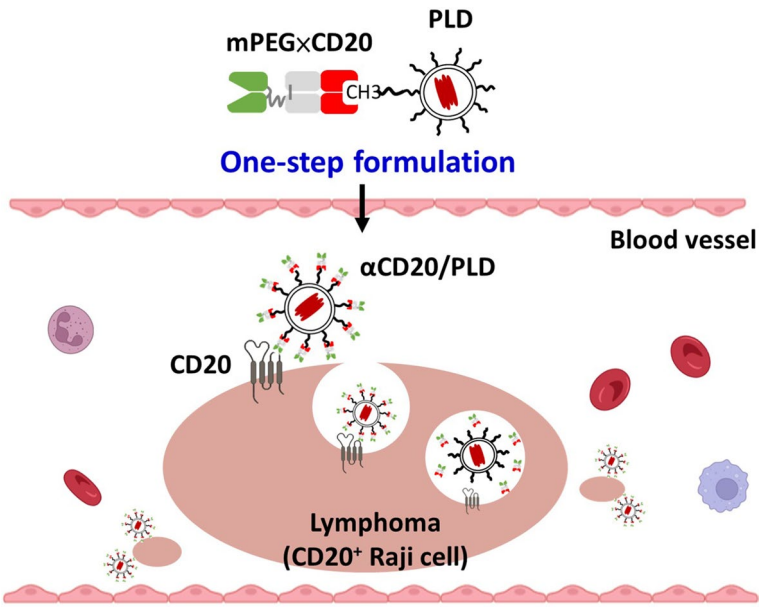

Fig. 1 Strategy by which the anti-PEG bispecific antibody (mPEG × CD20) targets PLD to CD20-expressing hematologic malignancies. The anti-PEG bispecific antibody (mPEG × CD20) can bind to the terminal methoxy groups present on PEG chains surrounding PLD and confer CD20 specificity to form αCD20/PLD. The αCD20/PLD can target to $CD20^+$ lymphoma Raji cells, enhancing internalization, and increasing anti-cancer activity in hematologic malignancies lacking an EPR effect

Materials and methods

Reagents, cells, and animals

PEGylated liposomal doxorubicin (PLD), clinical Lipo-Dox® (2 mg/mL pegylated liposomal doxorubicin HCl), was purchased from TTY BioPharm and PEGylated DOPC/CHOL liposomes labeled with DiD (Lipo-DiD) were purchased from FormuMax Scientific, (Sunnyvale, CA, USA). Both formulations have the same concentration of lipid (DSPC:Cholesterol:DSPE-PEG2000 = 3:2:0.3). Expi293F cells were cultured in Expi293 expression medium (Thermo Fisher Scientific) on shakers (25 mm shaking diameter) with a shake speed of 120 rpm in a humidified atmosphere of 8% CO_2 in air at 37 °C. Human Burkitt lymphoma cell lines, $CD20^+$ Raji cells, were from American Type Culture Collection (ATCC) and were cultured in RPMI1640 (Sigma-Aldrich) supplemented with 6 g/L HEPES, 2 g/L NaHCO3, 10% heat-inactivated BCS (HyClone), penicillin (100 U/mL), and streptomycin (100 mg/mL) at 37 °C in a humidified atmosphere of 5% CO2 in air. No authentication besides confirming surface expression levels of CD20 was performed by the authors. Healthy 3–6-week-old female SCID mice (CB17/lcr-Prkdcscid/CrlNarl) were purchased from the National Laboratory Animal Center, Taipei, Taiwan. All animal procedures were performed in accordance with the Guidelines for Care and Use of Laboratory Animals of Kaohsiung Medical University and approved by the institutional animal care and use committee (IACUC) of Kaohsiung Medical University (IACUC number: 105169).

Construction and expression of bispecific antibodies

Human bispecific antibodies were created by linking the C-terminus of an anti-methoxy PEG Fab (clone h15-2b) to an anti-CD20 scFv or anti-dansyl (anti-DNS, control group) scFv via a flexible peptide $(GGGGS)_3$ to form mPEG × CD20 and mPEG × DNS, respectively. The anti-CD20 scFv was constructed by linking the Ofatumumab (clone: 2F2) VH and VL domains with a linker $(GGGGS)_3$; the detailed description of BsAbs have been published (Kao et al. 2014). We used the Murine Ig k-chain V-J2-C (amino acid sequences: METDTLLLWVLLLWVPGSTG) as a signal peptide in front of the antibody for secretion via the endoplasmic reticulum (ER). Then, the VL-Ck and VH-CH1-linker-scFv domains were separated with an IRES in the pLJCX retroviral vector (BD Biosciences, San Diego, CA) to generate pLJCX-mPEG Fab-CD20-scFv-6His and pLJCX-mPEG Fab-DNS-scFv-6His plasmids. For protein production, plasmids were transfected into Epxi293F cells using ExpiFectamine and protocols provided by the manufacturer (Thermo Fisher Scientific). Transfected cells were grown at 37 °C in an atmosphere of 8% CO_2 in air while shaking at 120 rpm for 5 days. Supernatant was harvested by centrifugation at 3000 rpm for 5 min. Proteins were purified by Ni Sepharose High Performance (GE Healthcare, Little Chalfont, UK) and protein molecular weight was found by SDS-PAGE.

Bi-functional assay of mPEG × CD20 and mPEG × DNS BsAb

Ninety-six well plates were coated with 50 μg/ml of poly-D-lysine in PBS for 5 min at 37 °C, washed twice with deuterium-depleted water and then coated with 2×10^5 $CD20^+$ Raji cells per well. To fix cells, 2% paraformaldehyde was added, left for 5 min, and then

neutralized by 0.1 M glycine. The mPEG × CD20 or mPEG × DNS (20 μg/mL) were added to the wells at room temperature for 30 min. After extensive washing, 10 μg/mL of $mPEG_{2K}$-BSA was added to the wells for 30 min. After further extensive washing, the bound concentrations of $mPEG_{2K}$-BSA were determined by adding 10 μg/mL of 6-3 anti-PEG backbone antibody for 30 min and then adding 0.4 μg/mL of goat anti-mouse IgG Fc-HRP (Jackson ImmunoResearch Laboratories). The wells were washed and then ABTS substrate was added for 30 min before absorbance values at 405 nm were measured in a microplate reader (Biochrom, St Albans, United Kingdom).

Optimal ratio of mPEG × CD20 BsAb and PLD

mPEG × CD20 were mixed with PLD in PBS at 4 °C for 5 min to form αCD20/PLD. The molar ratios of mPEG to BsAb were 4:360, 8:360, 16:360, and 24:360. Based on a 100 nm liposome containing ∼ 80,000 phospholipid molecules and ∼ 4528 mPEG-DSPE (the molar ratio of DSPC: cholesterol: DSPE-PEG2000 = 3: 2: 0.3), the corresponding number of BsAbs per PLD was estimated to be 50, 100, 200, and 400, respectively. To quantify the nonconjugated BsAb in αCD02/PLD, αCD20/PLD at different ratios were incubated in mPEG-2K-BSA-coated 96-well plates at RT for 45 min. After extensive washing, the BsAb was detected by 0.4 μg/mL of goat anti-human Fab-HRP, and then ABTS substrate was added for 30 min before absorbance values at 405 nm were measured in a microplate reader. The BsAb-conjugation rate of αCD20/PLD was calculated as the total number of BsAb minus the number of nonconjugated BsAbs, and then divided by the total number of BsAbs. To examine the ability of PLD modified with various ratios of mPEG × CD20 to bind to lymphoma cells expressing CD20, Raji cells (2×10^5 cells per well) were seeded in a poly-D-lysine-coated 96-well plate overnight at 37 °C. After fixing the cells, 50 μg per mL of αCD02/PLD made with densities of BsAb on PLD of 50, 100, 200, and 400 BsAb/PLD were added to the wells at RT for 20 min. After extensive washing with PBS, the bound concentrations of PLD were determined by sequentially adding 10 μg per mL of 6-3 anti-PEG antibody for 1 h, washing with DMEM three times, and then adding 0.4 μg per mL of goat anti-mouse IgG Fc-HRP. The wells were washed three times with PBS and then ABTS substrate was added for 30 min before absorbance values at 405 nm were measured in a microplate reader. To further analyze CD20-specific targeting efficacy of optimized BsAb-modified PLD, serial dilutions of αCD20/PLD (with ratios of 200 BsAb/PLD) were incubated with Raji cells in poly-D-lysine-coated 96-well plates. PLD binding was measured as described above. On the basis of our previous studies, we confirmed the physical characteristics of BsAb/PLD. As detailed in prior research, we observed a slight increase in the particle size of BsAb/PLD compared to PLD (105 nm versus 98.8 nm), and the zeta potential of BsAb/PLD also experienced a minor negative increase in comparison to PLD (− 50.8 mA versus − 43.4 mA) (Kao et al. 2014). The results indicate that the formulation of BsAb/PLD led to a minor alteration in the particle size of PLD, without significantly affecting the particles' stability.

The membrane integrity and stability of PLD after mPEG × CD20 modification

To assess the membrane integrity and stability of αCD20/PLD, we utilized αCD20/PLD (with ratios of 200 BsAb/PLD), PLD, and PLD incubated with Triton X-100 as a positive control (Fritze et al. 2006). These samples were incubated at 4 °C or 37 °C for 1, 3, 6, and

12 h, respectively. The fluorescent signal of doxorubicin was measured with a microplate reader (excitation, 480 nm; emission, 550 nm; Biochrom, St Albans, United Kingdom). The results were calculated as percentage stability of PLD according to the following formula: release of doxorubicin (%) = 100 × (fluorescent signal of different groups/fluorescent signal of PLD in Triton X-100).

The specificity and internalization of αCD20-armed liposome against CD20$^+$ lymphoma cells

2×10^5 CD20$^+$ Raji cells and CD20$^-$ Molt-3 cells were incubated with 20 nM (200 μL) BsAbs for 1 h on ice. Unbound antibodies were removed by extensive washing in cold PBS containing 0.05% BSA, followed by the addition of 1 μM (200 μL) PEGylated Lipo-DiD for 1 h on ice. After removal of unbound PLD by extensive washing in cold PBS containing 0.05% BSA, the surface fluorescence of viable cells was measured on a FACScanflow cytometer (Merck Flow Cytometer, Guava easyCyte System). Internalization of αCD20/PLD into CD20$^+$ Raji cells was examined by adding 2 μg/mL of αCD20/PLD and αDNS/PLD in staining buffer (PBS containing 0.05% BSA) to 2×10^5 CD20$^+$ Raji cells for 40 min at 4 °C. After extensive washing with PBS, the cells were transferred to fresh culture medium and incubated for 3, 6 and 12 h at 37 °C. Control cells were incubated at 4 °C for 12 h. PLD on the surface of CD20$^+$ Raji cells was determined by sequential staining with 10 μg/mL 6-3 anti-PEG antibody for 30 min and 4 μg/mL goat anti-mouse IgG Fcγ-FITC (Jackson ImmunoResearch Laboratories). After extensive washing with PBS, the fluorescence of cells was measured on a FACScanflow cytometer.

Internalization imaging of αCD20/Lipo-DiD by confocal microscopy

Raji cells (1×10^5 cells per well) were seeded onto poly-D-lysine-coated glass slides at a concentration of 20 μg/mL and then washed by deuterium-depleted water. The buffer was then replaced with RPMI1640 medium supplemented with 10% FBS (culture medium) at 37 °C in a humidified atmosphere containing 5% CO2 for 24 h. The cells were incubated with 2 μM of LysoTracker Green DND-26 in RPMI (Sigma-Aldrich) to stain lysosomes for 40 min at 37 °C. After washing with PBS, the cells were incubated with 15 μg/mL of αCD20/Lipo-DiD, αDNS/Lipo-DiD, and a receptor-blocking group, Ofatumumab (anti-CD20 Abs) with αCD20/Lipo-DiD in fresh culture medium at 37 °C for 3 h or 6 h. Subsequently, the cells were fixed with 4% paraformaldehyde and covered by DAPI Fluoromount-G® (Southern Biotech) for fluorescence signal visualization. The fluorescence signals were captured using an Olympus FluoView 1000 confocal laser scanning microscope.

In vitro-specific cytotoxicity of αCD20/PLD against CD20$^+$ lymphoma cells

Raji cells (1×10^3 cells per well) were seeded in 96-well plates at 37 °C overnight. The cells were incubated with serum-free medium (control) or serial dilutions of αCD20/PLD, αDNS/PLD, or PLD (100 μL per well) at 37 °C for 12 h. The medium was replaced with fresh medium and the cell viability was measured with the ATPlite luminescence assay system (PerkinElmer, Waltham, MA) after incubation for 96 h. The results are expressed as percentage inhibition of luminescence as compared with untreated cells according to the following formula: cell viability (%) = 100 × (treated luminescence/

untreated luminescence). The standard deviation for each data point was averaged over four samples ($n = 3$).

Tumor accumulation and biodistribution of αCD20-armed liposome in vivo

SCID mice were injected with 5×10^6 Raji cells subcutaneously in the hind foot. Raji-tumor-bearing SCID mice were intravenously injected with 10 nmol αCD20/Lipo-DiD or αDNS/Lipo-DiD when the tumor size was about 200 mm^3. The fluorescent signal of Lipo-DiD was monitored by an IVIS spectrum optical imaging system (excitation, 750 nm; emission, 780 nm; PerkinElmer, Waltham, MA, USA) at 24, 48, and 72 h post-injection. The tumors and different organs (blood, heart, lung, liver, spleen, kidney, intestines, stomach, pancreas, tumor) of each group were collected at 72 h after Lipo-DiD injection. The region of interest (ROI) in tumors or different organ areas was drawn and analyzed with Living Image software version 4.2 (Caliper Life Sciences).

Therapeutic efficacy of αCD20/PLD in systemic Raji-bearing mice

SCID mice were injected via the tail vein with 5×10^6 Raji cells. One week later, mice were randomized into groups of 6–8 mice per group and intravenously injected with saline or 2 mg/kg of αCD20/PLD, αDNS/PLD, PLD, αCD20 BsAb twice weekly for 2 weeks, up to a total dose of 8 mg/kg doxorubicin. Raji cell progression was monitored weekly and the injections caused the mice to become paralyzed. Mice were killed at the onset of paralysis; otherwise, the mice were maintained until 100 days and considered to be long-term survivors. Data were analyzed using GraphPad Prism 6.0. Survival was compared using Log rank test. Statistical significance was set at $P < 0.05$.

Results

Characterization of mPEG × CD20 BsAb

We developed a bispecific antibody (BsAb) that can simultaneously bind to mPEG and CD20. We fused an anti-mPEG Fab fragment (humanized anti-mPEG antibody, 15-2b) and an anti-CD20 scFv via a flexible linker to generate mPEG × CD20. The mPEG × DNS was also constructed as a negative control by replacing the anti-CD20 scFv with an anti-dansyl (anti-DNS, control group) scFv, which can bind to the small chemical hapten dansyl that is not present on the surface of cancer cells (Fig. 2a). The DNA plasmids were transfected into Epxi293F cells, and the secreted protein was harvested and purified with Ni Sepharose High-Performance affinity media. SDS-PAGE analysis showed that the BsAbs were composed of a heavy scFv fragment (57 kDa) and a light fragment (27 kDa) under reducing conditions, and an 84 kDa disulfide-linked BsAb under non-reducing conditions (Fig. 2b). To examine whether mPEG × CD20 could simultaneously bind to mPEG and CD20, a sandwich cell-based ELISA was performed by immobilizing $CD20^+$ Raji cells on a 96-well cell culture plate, followed by subsequent incubation with mPEG × CD20 or mPEG × DNS, and then reaction with $mPEG_{2K}$-BSA, anti-PEG monoclonal Ab 6.3 and HRP-conjugated secondary Ab. As shown in Fig. 2C, only mPEG × CD20 but not mPEG × DNS had a dose-dependent higher signal of OD405 nm (Fig. 2c). These results indicate that mPEG × CD20 can simultaneously recognize the mPEG molecule and the CD20 antigen and provide CD20 tropism to PLD.

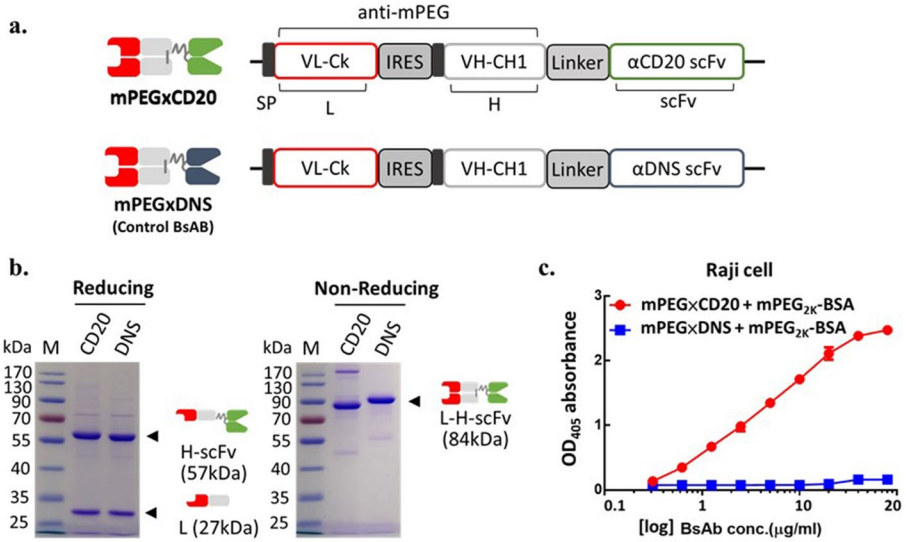

Fig. 2 Characterization of mPEG × CD20 BsAb **a** The gene constructs of BsAbs are composed of a signal peptide (SP), the anti-mPEG VL-C_k(L), the anti-mPEG VH-CH1(H), a flexible linker peptide and an anti-CD20 scFv (mPEG × CD20) or control anti-DNS scFv (mPEG × DNS). **b** The SDS-PAGE of purified mPEG × CD20 or mPEG × DNS under reducing and non-reducing conditions. M:pre-stained protein ladder. **c** The anti-mPEG and anti-CD20 functions of mPEG × CD20 and mPEG × DNS in $CD20^+$ Raji cells were detected via sandwich cell-based ELISA ($n = 3$). Bars, SD

Optimal modification of BsAbs for specific targeting of αCD20/PLD

To optimize the mPEG to BsAb modification ratio for PLD, mPEG × CD20 was mixed with PLD at BsAb densities on PLD of 50, 100, 200, and 400 BsAb/PLD. We confirmed that the conjugation rate of each BsAb on PLD was more than 85% (Additional file 1: Fig. S1a). To compare the binding ability of the different BsAb-modified αCD20/PLDs to $CD20^+$ Raji cells, we used sandwich cell-based ELISA which was performed by immobilizing $CD20^+$ Raji cells on a 96-well cell culture plate followed by subsequent incubation with different modified ratios with 50, 100, 200, and 400 BsAb/PLD. Then, we detected binding of BsAb/PLD with the anti-PEG backbone antibody (6-3 Ab) followed by HRP-conjugated secondary Ab (Additional file 1: Fig. S1b). The results show that 200 and 400 BsAb/PLD have higher binding affinity to $CD20^+$ Raji cells. To evaluate the optimized stability from 200 and 400 BsAb/PLD, we incubated these two formulations in PBS at 4 °C for 7 days, and found that the 400 BsAb/PLD had little precipitation compared to 200 BsAb/PLD. Thus, we demonstrated that the optimal modification of αCD20/PLD is 200 BsAb/PLD. To analyze whether mPEG × CD20 BsAb could impact the membrane integrity and stability of PLD, we incubated αCD20/PLD at BsAb densities of 200 BsAb/PLD at 4 °C or 37 °C for 1, 3, 6, and 12 and then measured the fluorescent signal of released doxorubicin. As shown in Additional file 2: Table S1, PLD displayed limited doxorubicin release: 0.9% at 4 °C for 6 and 12 h, 1.2% at 37 °C for 6 h, and 2.5% at 37 °C for 12 h. αCD20/PLD also exhibited minimal doxorubicin release: 0.7% at 4 °C for 6 h, 1.4% at 4 °C for 12 h, 2.7% at 37 °C for 6 h, and 3.9% at 37 °C for 12 h (Additional file 2: Table. S1). These results suggest that modification of mPEG × CD20 did not compromise the membrane integrity and stability of PLD.

αCD20-armed liposomes enhance targeting and cellular internalization of PLD to CD20$^+$ lymphoma cells

To investigate whether the αCD20/PLD specifically target CD20$^+$ Raji cells, αCD20/PLD were incubated with 2×10^5 CD20$^+$ Raji cells or CD20$^-$ Molt-3 cells for 1 h on ice, then the surface fluorescence of viable cells was measured on a FACScan flow cytometer. As shown in Fig. 3, αCD20/PLD had a higher fluorescence signal compared to αDNS/PLD in CD20$^+$ Raji cells, but in CD20$^-$ Molt-3 cells, no increased fluorescence signal was detected with either the αCD20/PLD or αDNS/PLD (Fig. 3a, b). These results suggest that αCD20/PLD is selective for CD20$^+$ lymphoma cells. To examine the internalization efficacy, we added 200 mPEG × CD20 per Lipo-DiD, which is a mPEGylated liposome that is labeled with a red fluorescent dye (DiD). The αCD20-armed liposomes were incubated with CD20$^+$ Raji cells for different time periods (3, 6, and 12 h). We detected total red fluorescence as a measure of the amount of DiD associated with cells (Fig. 3e). We also measured total liposomes present on the cell surface by measuring PEG by

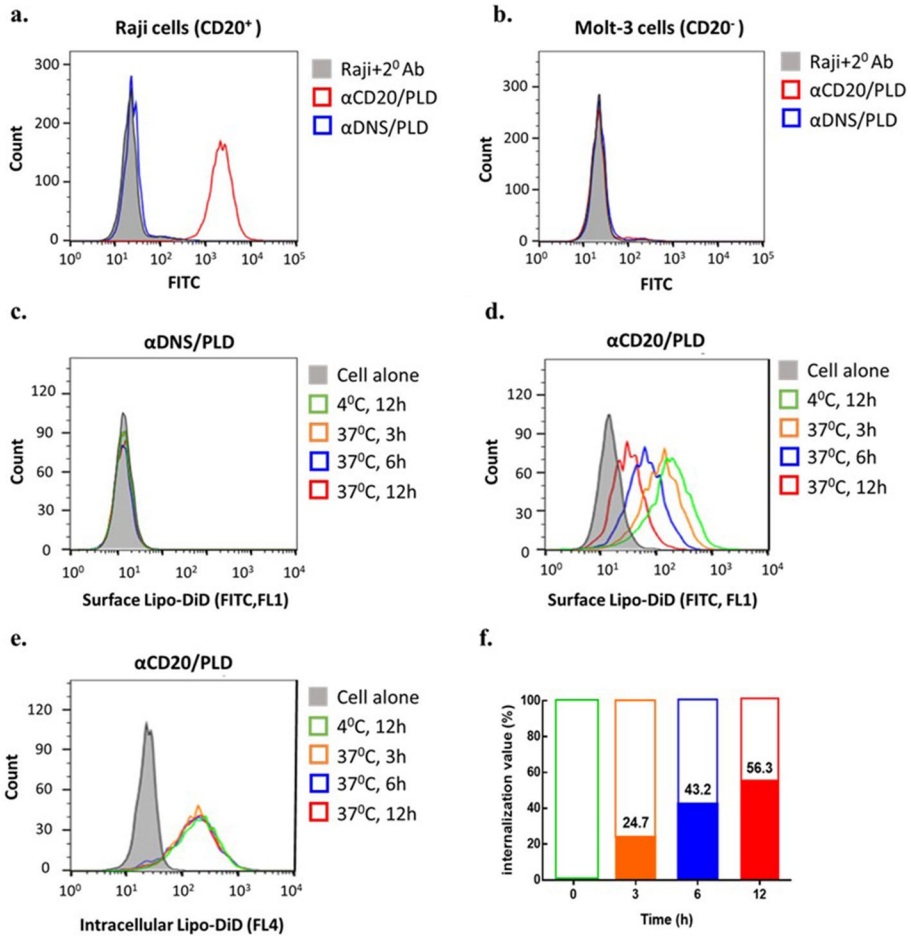

Fig. 3 αCD20-armed liposomes enhance selection and internalization of PLD against CD20 + lymphoma cells. **a** αCD20/PLD (red) and αDNS/PLD (blue) were incubated with CD20 + Raji cells and **b** CD20- Molt-3 cells. The particles were measured using flow cytometry with an anti-PEG antibody. **c** The internalization of αDNS/PLD and **d** αCD20/PLD into Raji cells. The surface Lipo-DiD was measured using flow cytometry with an anti-PEG antibody. **e** The DiD uptake of αCD20/PLD in Raji cells was detected using flow cytometry. **f** The internalization values (%) were determined at different time intervals of incubation

staining with 6-3 antibody (anti-PEG backbone) and anti-mouse Fc Ab-FITC. As shown in Fig. 3B, the red fluorescence signal was at a similar level at different times, showing that liposomes were associated with cells, but the green fluorescence signal gradually decreased in a time-dependent manner after incubation with Lipo-DiD, showing that liposomes internalized. The internalization value of αCD20-armed liposomes at 12 h was up to 56.3%, at 6 h was 43.2% and at 3 h it was only 24.7% (Fig. 3c, d, f). These results indicate that αCD20-armed liposome can specifically target $CD20^+$ lymphoma cells and efficiently trigger internalization.

mPEG × CD20 BsAb enhances the internalization of Lipo-DiD by receptor-mediated endocytosis

To investigate whether mPEG × CD20 BsAb can specifically enhance the internalization of mPEGylated particles into tumor cells by CD20-mediated endocytosis, Raji (CD20-overexpressing) cells were incubated with αCD20/Lipo-DiD, αDNS/Lipo-DiD, and a receptor-blocking group, Ofatumumab (anti-CD20 Abs) with αCD20/Lipo-DiD in fresh culture medium at 4 °C for 30 min and 37 °C for 3 h or 6 h. Subsequently, the fluorescence signals of Lipo-DiD were detected by confocal microscopy imaging. DAPI and Lysotracker Green were used to stain the nuclei and lysosomes, respectively. Results in new Fig. 4 show red fluorescence signals (Lipo-DiD) detected in the αCD20/Lipo-DiD group, indicating specific binding to Raji cells. Additionally, red Lipo-DiD signals progressively transitioned from the plasma membrane to the cytoplasm, co-localizing with green lysosomal signals, forming yellow in the αCD20/Lipo-DiD group. This observation suggests successful internalization of Lipo-DiD into Raji cells. In contrast, pre-incubation with competitor Ofatumumab (anti-CD20 Abs) prevented uptake of αCD20/Lipo-DiD, indicating the function of mPEG × CD20 BsAbs could be competed with αCD20 Ab (Fig. 4). These results suggested that mPEG × CD20 BsAb can selectively bind and enhance the internalization of mPEG-liposomes (Lipo-DiD) through CD20-mediated endocytosis, which is crucial for increasing the cellular nanoparticles uptake.

αCD20/PLD displays cytotoxicity to $CD20^+$ lymphoma cells

To analyze the cytotoxicity of αCD20/PLD to CD20-overexpressing Raji cells, we incubated $CD20^+$ Raji cells with different concentrations of αCD20/PLD, αDNS/PLD, or PLD for 12 h, then removed the drug, and washed the cells. The cell viability was determined by ATPlite assay 96 h post-drug treatment. The results are expressed as percentage inhibition as compared with untreated cells according to the following formula: cell viability (%) = 100 × (treated signal/untreated signal). As shown in Fig. 4, αCD20/PLD (IC_{50} = 0.071 μg/mL) significantly reduced the cell viability of Raji cells as compared with αDNS/PLD (IC_{50} = 0.92 μg/mL) and PLD (IC_{50} = 1.08 μg/mL) (Fig. 5a, b). These results show that bispecific antibody targeting improved the cytotoxicity of αDNS/PLD to $CD20^+$ Raji cells by 15-fold.

Specific targeting and tumor accumulation of αCD20-armed liposomes in Raji-bearing SCID mice

To examine the specific targeting and tumor accumulation of αCD20/PLD to CD20-overexpressing B-cell lymphoma tumors in vivo, we established a human B-cell

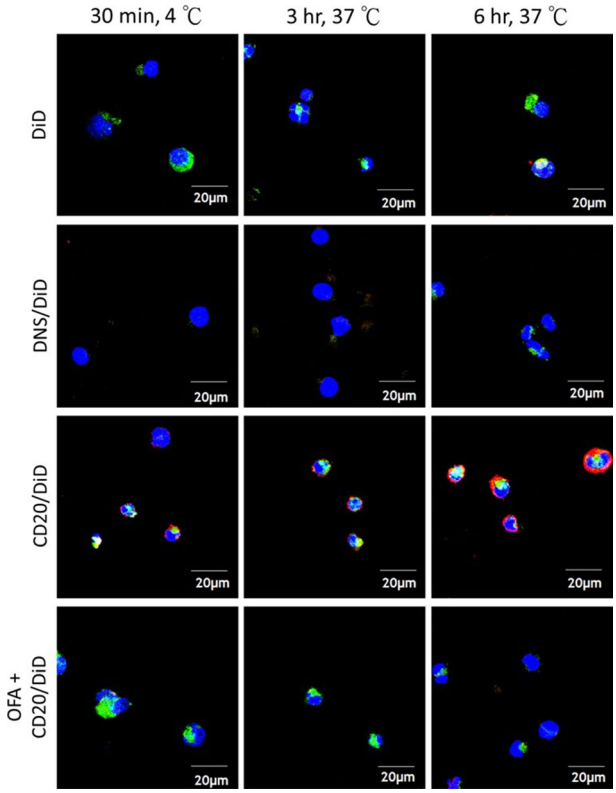

Fig. 4 mPEG × CD20 BsAb enhances the internalization of Lipo-DiD by receptor-mediated endocytosis. Raji cells were incubated with αCD20/Lipo-DiD, αDNS/Lipo-DiD, and a receptor-blocking group, Ofatumumab (anti-CD20 Abs), in combination with αCD20/Lipo-DiD. This was followed by supplementation with DAPI and LysoTracker Green DND-26 and the samples were observed using a confocal microscope. DAPI (blue), LysoTracker Green DND-26 (green), and Lipo-DiD (red) stain for the nuclei, lysosome, and Lipo-DiD, respectively. White scale bars represent 20 μm

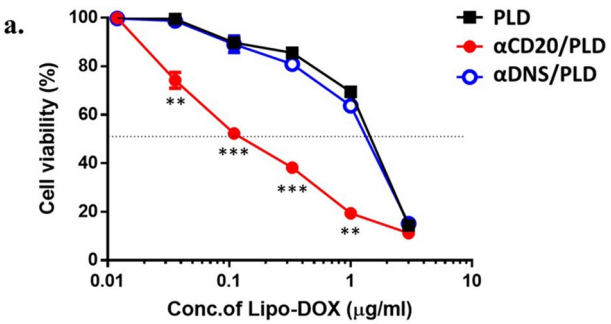

b.

	PLD	αCD20/PLD	αDNS/PLD
IC_{50} (μg/ml)	1.079	0.071	0.921

Fig. 5 The cytotoxicity of αCD20/PLD against $CD20^+$ lymphoma cells. **a** PLD (▩), αCD20/PLD (●) or αDNS/PLD (○) were incubated with $CD20^+$ lymphoma cells for 12 h. The cell viability was determined by ATPlite analysis and the mean luminescence values were compared to untreated control cells ($n = 3$). Bars, SD. **b** The half-maximal inhibitory concentration (IC50) values of PLD, αCD20/PLD or αDNS/PLD. Bars, SD. $^*P < 0.05$. $^{**}P < 0.01$.; *n.s.* not significant

lymphoma carcinoma xenograft model by subcutaneously inoculating $CD20^+$ Raji cells in the hind foot of SCID mice. When the tumor size reached ~ 250 mm^3, we intravenously injected αCD20/Lipo-DiD or αDNS/Lipo-DiD, respectively. The red fluorescent signal of Lipo-DiD was detected by an IVIS imaging system at 24, 48, and 72 h post-injection. The images showed that αCD20/Lipo-DiD had more intense fluorescence accumulation as compared to αDNS/DiD. The region of interest (ROI) in αCD20/Lipo-DiD-treated tumors increased by 290% (17.2×10^9 versus 6×10^9), 280% (15.1×10^9 versus 5.4×10^9), and 295% (12.1×10^9 versus 4.1×10^9) at 24, 48, and 72 h, respectively, as compared with αDNS/Lipo-DiD (Fig. 6a, b). These results indicate the αCD20/Lipo-DiD can more specifically target to $CD20^+$ B-cell lymphoma tumors. To analyze the biodistribution of αCD20/Lipo-DiD, the mice were killed 72 h post-injection and the organs (blood, heart, lung, liver, spleen, kidney, intestines, stomach, pancreas, tumor) were collected. αCD20/Lipo-DiD had up to 2.8-fold signal accumulation as compared to αDNS/Lipo-DiD in tumors, and had lower uptake in metabolic organs such as the lung, liver, and spleen (Fig. 6c). These results indicate that αCD20-armed liposomes preferentially accumulate in tumor tissue.

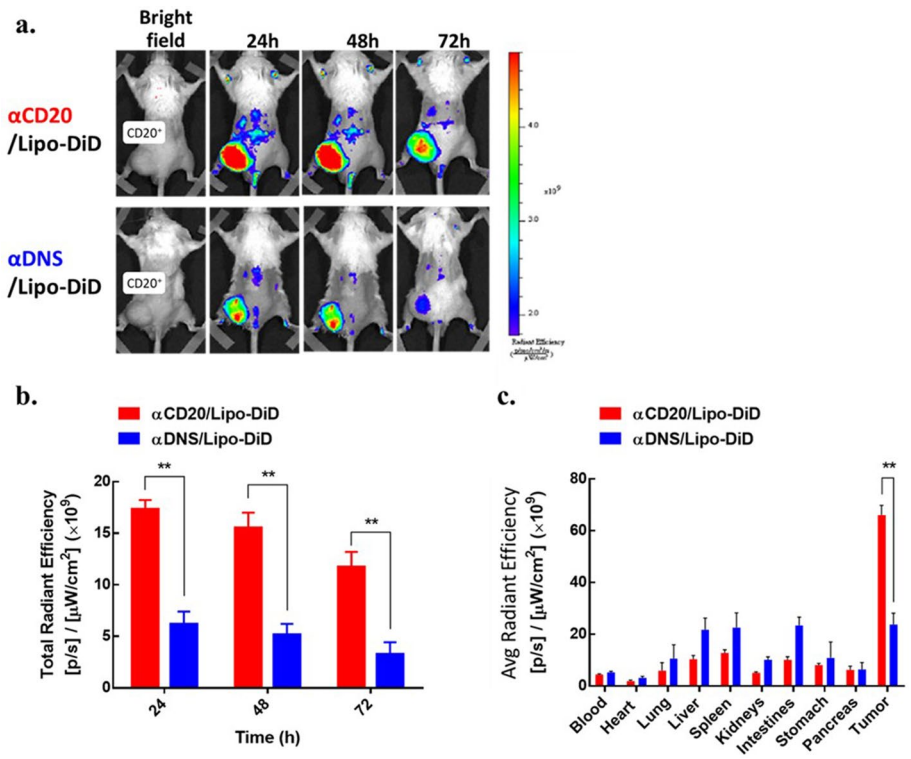

Fig. 6 Tumor delivery of αCD20-armed liposomes in Raji-bearing SCID mice. **a** αCD20/Lipo-DiD or αDNS/Lipo-DiD were intravenously injected into SCID mice bearing $CD20^+$ tumors (left flank). The fluorescence intensity of DiD was detected at 24 h, 48 h, and 72 h after injection by IVIS. **b** Total radiant efficiency of αCD20/Lipo-DiD (red) or αDNS/Lipo-DiD (blue) in $CD20^+$ tumors and **c** the average radiant efficiency of the collected organs and tumors at 72 h were quantified ($n = 3$). Bars, SEM. $^{**}P < 0.01$. $^{*}P < 0.05$; *n.s.* not significant

αCD20/PLD increases the therapeutic efficacy of PLD in a systemic Raji-tumor SCID mouse model

To investigate the therapeutic efficacy of αCD20/PLD to $CD20^+$ lymphoma tumors in vivo, we established a systemic Raji-tumor model in SCID mice. SCID mice were injected via the tail vein with 5×10^6 $CD20^+$ Raji cells. One week later, mice were intravenously treated with saline, 2 mg/kg of αCD20/PLD, αDNS/PLD, PLD, or αCD20 BsAb twice a week for 2 weeks and paralysis was observed and body weight was measured twice a week. The mice which were not paralyzed were maintained for 100 days. Mice in the non-treated and αCD20 BsAb groups all died by day 42, whereas mice treated with αDNS/PLD or PLD died between days 80 and 90. There was no significant difference between the αDNS/PLD- and PLD-treated groups, but in the αCD20/PLD group, 90% survival rate was extended until 100 days ($P < 0.0001$) (Fig. 7a). These results show that αCD20/PLD can increase anti-tumor and therapeutic efficacy of PLD in a systemic Raji-tumor SCID mouse model in vivo. There was no significant change in the body weight of mice in each treatment group (Fig. 7b). These results demonstrate that αCD20/PLD can enhance the therapeutic efficacy of PLD in CD20-overexpressing B-cell lymphoma cancer with minimal obvious toxicity.

Discussion

In this study, we successfully modified mPEG × CD20 BsAb on PLD to provide a targeted treatment method for lymphoma. mPEG × CD20 conferred CD20 specificity to PLD through a one-step formulation without affecting PLD production, and effectively promoted the internalization of PLD into Raji cells. αCD20/PLD displayed increased cytotoxicity of about 15-fold compared with PLD alone to $CD20^+$ Raji cells. Moreover, αCD20/PLD specifically targeted Raji tumors and decreased the non-specific targeting to normal tissues; mice treated with αCD20/PLD reached 90% survival rate at 100-day post-injection. Our results show that an anti-mPEG BsAb combined with PEG-NPs can actively crosslink surface tumor-associated antigens and enhance nanoparticle endocytosis. Moreover, the tumor specificity of the BsAb is exchangeable to overcome antibody-resistant tumors which lose the marker on the surface of tumor cells through antibody treatment. Thus, anti-mPEG BsAb-modified PEG-NPs are more effective at systemic targeting, internalization and the anti-tumor efficacy in hematologic malignancies.

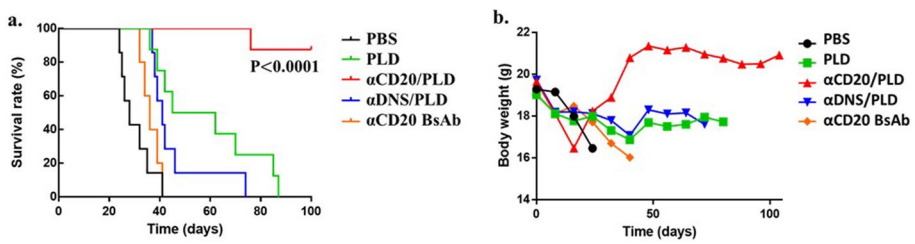

Fig. 7 Therapeutic efficacy of αCD20/PLD BsAbs in a systemic Raji-tumor SCID mouse model. SCID mice bearing Raji cells were intravenously injected with 2 mg per kg of αCD20/PLD (red, $n = 8$), αDNS/PLD (blue, $n = 7$), PLD (green, $n = 8$), αCD20 BsAb (orange, $n = 5$) or PBS (black, $n = 7$). Treatment was performed twice a week for 2 weeks. **a** Percentage survival as mean and **b** the mean of body weight were measured every 3 days post-treatment. Bars, SEM. $^{**}P < 0.01$. $^{*}P < 0.05$; *n.s.* not significant

Antibody-mediated cross-linking of antigens can enhance the endocytic capacity into cancer cells and further increase the uptake and therapeutic effect of the drug. For example, Li and colleagues conjugated one or ten anti-CD20 Fab molecules on a polymeric nanomedicine and showed that the particles with higher levels of anti-CD20 Fab displayed enhanced internalization in Raji cells by 2.7-fold as compared with the nanoparticles conjugated with a single anti-CD20 Fab (Li et al. 2018). They also found that multiple anti-CD20 Fab on nanoparticles significantly increased cellular apoptosis, indicating that cross-linking CD20 can directly induces apoptosis of lymphoma B cells (Chu et al. 2015). However, binding of antibodies to different epitopes on the CD20 antigen can influence internalization (Klein et al. 2013). Ofatumumab is the only anti-CD20 antibody that binds the small extracellular loop of CD20 close to the surface of the cell membrane, resulting in cross-linking of CD20 and enhancing internalization (Du et al. 2009; Davis et al. 1999; Zhou et al. 2008). Ofatumumab can induce about two-fold greater internalization than rituximab (Beum et al. 2011; Herter et al. 2013). Thus, we used ofatumumab to generate the mPEG × CD20 bispecific antibody. The mPEG × CD20 bispecific antibody (BsAb) was mixed with PLD to generate the multivalent anti-CD20 nanoparticle (αCD20/PLD), which had approximately 100 BsAbs per liposome. αCD20/PLD exhibited about 56-fold greater internalization and 15-fold increased cytotoxicity in Raji cells as compared with untargeted PLD. Modification of mPEG × CD20 also significantly enhanced accumulation in Raji tumors by 2.8-fold in comparison with mPEG × DNS-conjugated PEGylated liposomal DiD. Moreover, αCD20/PLD had significantly greater therapeutic efficacy as compared to PLD ($P < 0.0001$), resulting in a 90% long-term survival rate. Therefore, anti-PEG bispecific antibodies can cross-linking antigens to improve endocytosis and therapeutic effect of PEG-NP in hematologic malignancies.

Solving the drug-resistance issue is important for lymphoma patients who receive long-term chemotherapy. A doxorubicin-based chemotherapy, CHOP, is the most effective treatment for high-grade B-cell lymphoma, but about 20–30% patients acquire doxorubicin-resistance and lowered survival rate with this protocol (Nagashima, et al. 2016; Kao et al. 2014). Liu et al. found that using mPEGylated liposomal-irinotecan (Onivyde) to replace mPEGylated liposomal doxorubicin (Lipo-Dox) enhanced cytotoxicity 33.5-fold in doxorubicin-resistance recurrent ovarian cancer cells (Murawski et al. 2010; O'Brien et al. 2004). Tadahiro et al. reported that Onivyde improved the survival of mice with doxorubicin-resistant acute lymphoblastic leukemia as compared to Lipo-Dox treatment in vivo. Pegylated nanomedicines such as Lipo-Dox (Zaja et al. 2006; Murawski et al. 2010), Onivyde (Cheng et al. 2020; Kao et al. 2014), and PEGylated liposomal-Mitomycin C (PROMITIL) are being used or under clinical trials for cancer treatment (Cheng et al. 2020). The PEG × CD20 BsAb is able to bind to any terminal methoxy groups of PEG-NPs to confer CD20 specificity, which can facilitate switching of the nanomedicine in patients who develop drug resistance to a particular drug.

Several reports report that lymphoma cells lose cell surface antigens after antibody treatment, leading to drug resistance. For example, the response rate of re-treatment of rituximab is lower than 50% (Davis et al. 2000). Furthermore, Kennedy found that 60% of patients who received rituximab had lost CD20 expression (Kennedy et al. 2002), and this phenomenon extended to loss of CD19 (Masir et al. 2006). Antigen loss after targeted treatment has also been reported in CAR-T therapies. Eleven–twenty-five percent

of patients who receive CD19 CAR-T therapies relapse with leukemia without CD19. Thus, how to conveniently convert the antigen targeting of the drug is important. Caratelli and colleagues generated Fcγ chimeric receptor-expressing CAR-T cells, and the Fcγ receptor-expressing CAR-T was able to capture different therapeutic antibodies to provide several tumor-associated antigen (TAA)-specific targeting treatment (Caratelli et al. 2017). Landgraf and colleagues generated NKG2D receptor-expressing CAR-T cells, and fused its MIC ligand on rituximab, and they demonstrated that injection of NKG2D CAR-T cells and MIC-rituximab could enhance the survival rate of Raji-bearing mice. For the nanodrugs, we generated anti-PEG BsAbs (mPEG × markers), which can convert the TAA (such as CD20, CD19, CD22, and CD52) target using different anti-tumor scFv. The anti-PEG BsAbs can confer the PEG-NP with various antigen targeting specificity against the heterogenic lymphoma. According to the specific antigens expressed on the cancer cells of the patients, we can select the anti-PEG BsAbs that correspond to the specific antigen expressed on the cancer cells of the patient, and then directly mix it in one-step with PEG-NP to treat the patient. Thus, anti-PEG BsAbs can provide a convertible therapeutic strategy which can adjust antigen specificity for treating antigen loss in lymphoma.

Conclusion

In summary, the non-covalent modification of liposomes with mPEG × CD20 provides a simple and stable one-step formulation for site-specific modification of PEG-NPs, aiming to enhance drug internalization and therapeutic efficacy of PLD. This approach achieved a remarkable 90% survival rate at 100-day post-treatment in the systemic tumor SCID mouse model. Thus, this study represents the pioneering use of targeted nanomedicine for the treatment of hematologic malignancies, addressing their deficiency in the EPR effect. We suggest that the BsAb-modifying strategy has the following advantages and potential: (i) it is a novel and simple modification method to replace the traditional chemical conjugation; (ii) it has exchangeable properties and universal applicability, and BsAbs can directly diversify PEG-NPs to different biomarkers expressed in individual diseases for diagnosis and therapy; and (iii) the BsAb modification can increase antigen cross-linking and enhance the internalization of PEG-NPs to improve the anti-cancer effect. We conclude that BsAbs (mPEG × markers) can expand the clinical application of PEG-NPs for treating hematologic malignancies lacking the EPR effect via improved tumor-specific targeting, internalization, and, thus, improved therapeutic efficacy.

Supplementary Information

The online version contains supplementary material available at https://doi.org/10.1186/s12645-023-00230-6.

Additional file 1: Fig. S1. Optimization of mPEG × CD20 BsAb-modified PLD. **a**. The CD20 conjugated ratio of αCD2/PLD with densities of BsAb on PLD of 400, 200, 100, and 50 BsAb/PLD was investigated via ELISA ($n = 3$). Bars, SD. *b*. The CD20 binding ability of αCD20/PLD with different ratio (400, 200, 100, and 50 BsAb/PLD) on $CD20^+$ lymphoma cells was determined via ELISA ($n = 3$). Bars, SD.

Additional file 2: Table S1. Release of doxorubicin from PLD and αCD20/PLD. αCD20/PLD (with ratios of 200 BsAb/PLD), PLD, and PLD incubated with Triton X-100 were subjected to incubation at 40c or 370c for 1, 3, 6, and 12 h, respectively, followed by the measurement of fluorescent release of doxorubicin. The release of doxorubicin values was calculated as a percentage during various incubation times.

Author contributions
H-JC designed and performed experiments reported in the paper, analyzed data and wrote the manuscript; Y-AC helped with experiments, data analysis, and contributed to manuscript editing; Y-TC and C-CL help the internalization experiments, data analysis for internalization; B-CH and S-TH provided the information of leukemia clinical treatments and current challenges; I-JC and K-WH help the animal experiments; C-YC, F-MC, J-YW and SRR provided the concept and contributed to manuscript writing and editing; T-LC and D-HW provided the concept, experimental design, and contributed to manuscript writing and editing.

Funding
This work was supported by grants from the Ministry of Science and Technology, Taipei, Taiwan (MOST 110-2320-B-037 -010 -MY3, MOST 111-2124-M-037-001-MY3, MOST 111-2314-B-037 -051 -MY3, MOST 111-2314-B-037-094-MY3); the KMU-KMUH Co-Project of Key Research (KMUH-DK(B)110004-3, KMUH-DK(B)110006-1, KMUH-DK(B)110006-2, KMUH-DK(B)111004-2, KMUH-DK(B)111001-3, KMUH-DK(B)112001-2) and Research Foundation (KMU-DK(B)110004-2, KMU-DK(B)111004, KMU-DK(B)111001-2, KMU-DK(B)112001-1, KMU-DK(B)112001-3) from Kaohsiung Medical University, Kaohsiung, Taiwan. This work was also supported partially by Kaohsiung Medical University Research Center Grant (Drug Development and Value Creation Research Center) (KMU-TC112A03); NTHU-KMU Joint Research Project (KT112P002).

Availability of data and materials
All data underlying the results are available as part of the article and no additional source data are required.

Declarations

Ethics approval and consent to participate
Not applicable.

Consent for publication
The authors consent for publication.

Competing interests
The authors declare no competing interests.

Author details
[1]Department of Biomedical Science and Environmental Biology, Kaohsiung Medical University, 100 Shih-Chuan 1st Road, Kaohsiung 80708, Taiwan. [2]Graduate Institute of Medicine, College of Medicine, Kaohsiung Medical University, Kaohsiung, Taiwan. [3]Drug Development and Value Creation Research Center, Kaohsiung Medical University, Kaohsiung, Taiwan. [4]Department of Medical Research, Kaohsiung Medical University Hospital, Kaohsiung, Taiwan. [5]Department of Medical Imaging, Kaohsiung Medical University Hospital, Kaohsiung, Taiwan. [6]School of Post-Baccalaureate Medicine, College of Medicine, Kaohsiung Medical University, Kaohsiung, Taiwan. [7]Division of Breast Oncology and Surgery, Department of Surgery, Kaohsiung Medical University Hospital, Kaohsiung, Taiwan. [8]Department of Surgery, Kaohsiung Municipal Ta-Tung Hospital, Kaohsiung, Taiwan. [9]Department of Surgery, Faculty of Medicine, College of Medicine, Kaohsiung Medical University, Kaohsiung, Taiwan. [10]Institute of Biomedical Sciences, Academia Sinica, Taipei, Taiwan. [11]Chia Nan University of Pharmacy and Science, 60 Section 1, Erren Rd, Rende District, Tainan 71710, Taiwan. [12]School of Medicine, I-Shou University, Kaohsiung, Taiwan.

Received: 7 June 2023 Accepted: 15 September 2023
Published online: 06 October 2023

References

Bendas G et al (1999) Targetability of novel immunoliposomes prepared by a new antibody conjugation technique. Int J Pharm 181(1):79–93
Beum PV et al (2011) Loss of CD20 and bound CD20 antibody from opsonized B cells occurs more rapidly because of trogocytosis mediated by fc receptor-expressing effector cells than direct internalization by the B cells. J Immunol 187(6):3438
Caratelli S et al (2017) FCγ chimeric receptor-engineered T cells: methodology, advantages, limitations, and clinical relevance. Front Immunol 8:457–457
Chatterjee K et al (2010) Doxorubicin cardiomyopathy. Cardiology 115(2):155–162
Cheng YA et al (2019) Enhanced drug internalization and therapeutic efficacy of PEGylated nanoparticles by one-step formulation with anti-mPEG bispecific antibody in intrinsic drug-resistant breast cancer. Biomater Sci 7(8):3404–3417
Cheng YA et al (2020) Humanized bispecific antibody (mPEG × HER2) rapidly confers PEGylated nanoparticles tumor specificity for multimodality imaging in breast cancer. J Nanobiotechnol 18(1):118
Chu TW et al (2015) A two-step pretargeted nanotherapy for CD20 crosslinking may achieve superior anti-lymphoma efficacy to rituximab. Theranostics 5(8):834–846
Coiffier B, Sarkozy C (2016) Diffuse large B-cell lymphoma: R-CHOP failure-what to do? Hematology. Am Soc Hematol Educ Program 2016(1):366–378
Coiffier B et al (2010) Long-term outcome of patients in the LNH-985 trial, the first randomized study comparing rituximab-CHOP to standard CHOP chemotherapy in DLBCL patients: a study by the Groupe d'Etudes des Lymphomes de l'Adulte. Blood 116(12):2040–5

Da-Silva-Freitas D et al (2015) PEGylation: a successful approach to improve the biopharmaceutical potential of snake venom thrombin-like serine protease. Protein Pept Lett 22(12):1133–1139
Davis TA et al (1999) Therapy of B-cell lymphoma with anti-CD20 antibodies can result in the loss of CD20 antigen expression. Clin Cancer Res 5(3):611–615
Davis TA et al (2000) Rituximab anti-CD20 monoclonal antibody therapy in non-Hodgkin's lymphoma: safety and efficacy of re-treatment. J Clin Oncol 18(17):3135–3143
Du J et al (2009) Structure of the Fab fragment of therapeutic antibody Ofatumumab provides insights into the recognition mechanism with CD20. Mol Immunol 46(11):2419–2423
Franco YL et al (2018) Anticancer and cardio-protective effects of liposomal doxorubicin in the treatment of breast cancer. Breast Cancer 10:131–141
Fritze A et al (2006) Remote loading of doxorubicin into liposomes driven by a transmembrane phosphate gradient. Biochim Biophys Acta 1758:1633–1640
García-Noblejas A, et al. (2018) Liposomal doxorubicin in aggressive B cell lymphoma shows similar efficacy to the conventional formulation: long term results from a retrospective cohort study. European Hematology Association, Poster Presentation 215360; PS1038
Hammer MK et al (2007) A novel enzyme complementation-based assay for monitoring G-protein-coupled receptor internalization. FASEB J 21(14):3827–3834
Herter S et al (2013) Preclinical activity of the type II CD20 antibody GA101 (Obinutuzumab) compared with rituximab and Ofatumumab in vitro and in xenograft models. Mol Cancer Ther 12(10):2031–2042
Huwyler J et al (2008) Tumor targeting using liposomal antineoplastic drugs. Int J Nanomed 3(1):21–29
Jardin F et al (2019) Improving R-CHOP in diffuse large B-cell lymphoma is still a challenge. Lancet Oncol 20(5):605–606
Jiang S et al (2016) CD20 monoclonal antibody targeted nanoscale drug delivery system for doxorubicin chemotherapy: an in vitro study of cell lysis of CD20-positive Raji cells. Int J Nanomed 11:5505–5518
Kao CH et al (2014) One-step mixing with humanized anti-mPEG bispecific antibody enhances tumor accumulation and therapeutic efficacy of mPEGylated nanoparticles. Biomaterials 35(37):9930–9940
Kennedy GA et al (2002) Incidence and nature of CD20-negative relapses following rituximab therapy in aggressive B-cell non-Hodgkin's lymphoma: a retrospective review. Br J Haematol 119(2):412–416
Khan DR et al (2015) Use of targeted liposome-based chemotherapeutics to treat breast cancer. Breast Cancer 9(Suppl 2):1–5
Klein C et al (2013) Epitope interactions of monoclonal antibodies targeting CD20 and their relationship to functional properties. Mabs 5(1):22–33
Li L et al (2018) Amplification of CD20 cross-linking in rituximab-resistant B-lymphoma cells enhances apoptosis induction by drug-free macromolecular therapeutics. ACS Nano 12(4):3658–3670
Manjappa AS et al (2011) Antibody derivatization and conjugation strategies: application in preparation of stealth immunoliposome to target chemotherapeutics to tumor. J Control Release 150(1):2–22
Masir N et al (2006) Loss of CD19 expression in B-cell neoplasms. Histopathology 48(3):239–246
Milla P et al (2012) PEGylation of proteins and liposomes: a powerful and flexible strategy to improve the drug delivery. Curr Drug Metab 13(1):105–119
Murawski N et al (2010) Unresolved issues in diffuse large B-cell lymphomas. Expert Rev Anticancer Ther 10(3):387–402
Nagashima K et al (2016) Immune pancytopenia after chemotherapy in a patient with diffuse large B-cell lymphoma. BMJ Case Rep. https://doi.org/10.1136/bcr-2016-216880
Nobs L et al (2004) Current methods for attaching targeting ligands to liposomes and nanoparticles. J Pharm Sci 93(8):1980–1992
O'Brien MER et al (2004) Reduced cardiotoxicity and comparable efficacy in a phase III trial of pegylated liposomal doxorubicin HCl(CAELYX™/Doxil®) versus conventional doxorubicin for first-line treatment of metastatic breast cancer. Ann Oncol 15(3):440–449
Oki Y et al (2015) Pegylated liposomal doxorubicin replacing conventional doxorubicin in standard R-CHOP chemotherapy for elderly patients with diffuse large B-cell lymphoma: an open label, single arm, phase II trial. Clin Lymphoma Myeloma Leuk 15(3):152–158
Rivankar S et al (2014) An overview of doxorubicin formulations in cancer therapy. J Cancer Res Ther 10(4):853–858
Sapra P et al (2002) Internalizing antibodies are necessary for improved therapeutic efficacy of antibody-targeted liposomal drugs. Cancer Res 62(24):7190–7194
Shahum E et al (1998) Immunopotentiation of the humoral response by liposomes: encapsulation versus covalent linkage. Immunology 65:315–317
Suk JS et al (2016) PEGylation as a strategy for improving nanoparticle-based drug and gene delivery. Adv Drug Deliv Rev 99:28–51
Trubetskoy VS et al (1992) Use of N-terminal modified poly(L-lysine)-antibody conjugate as a carrier for targeted gene delivery in mouse lung endothelial cells. Bioconjug Chem 3(4):323–327
Tsimberidou AM et al (2010) Ofatumumab in the treatment of chronic lymphocytic leukemia. Drugs Today 46(7):451–461
Wu C et al (2014) Potentiating antilymphoma efficacy of chemotherapy using a liposome for integration of CD20 targeting, ultra-violet irradiation polymerizing, and controlled drug delivery. Nanoscale Res Lett 9(1):447
Zaja F et al (2006) CHOP-rituximab with pegylated liposomal doxorubicin for the treatment of elderly patients with diffuse large B-cell lymphoma. Leuk Lymphoma 47(10):2174–2180
Zhang R et al (2016) Nanomedicine of synergistic drug combinations for cancer therapy—strategies and perspectives. J Control Release 240:489–503
Zhou X et al (2008) The role of complement in the mechanism of action of rituximab for B-cell lymphoma: implications for therapy. Oncologist 13(9):954–966

Publisher's Note